1. SUPPLEMENTARY FIGURES

Figure S1.

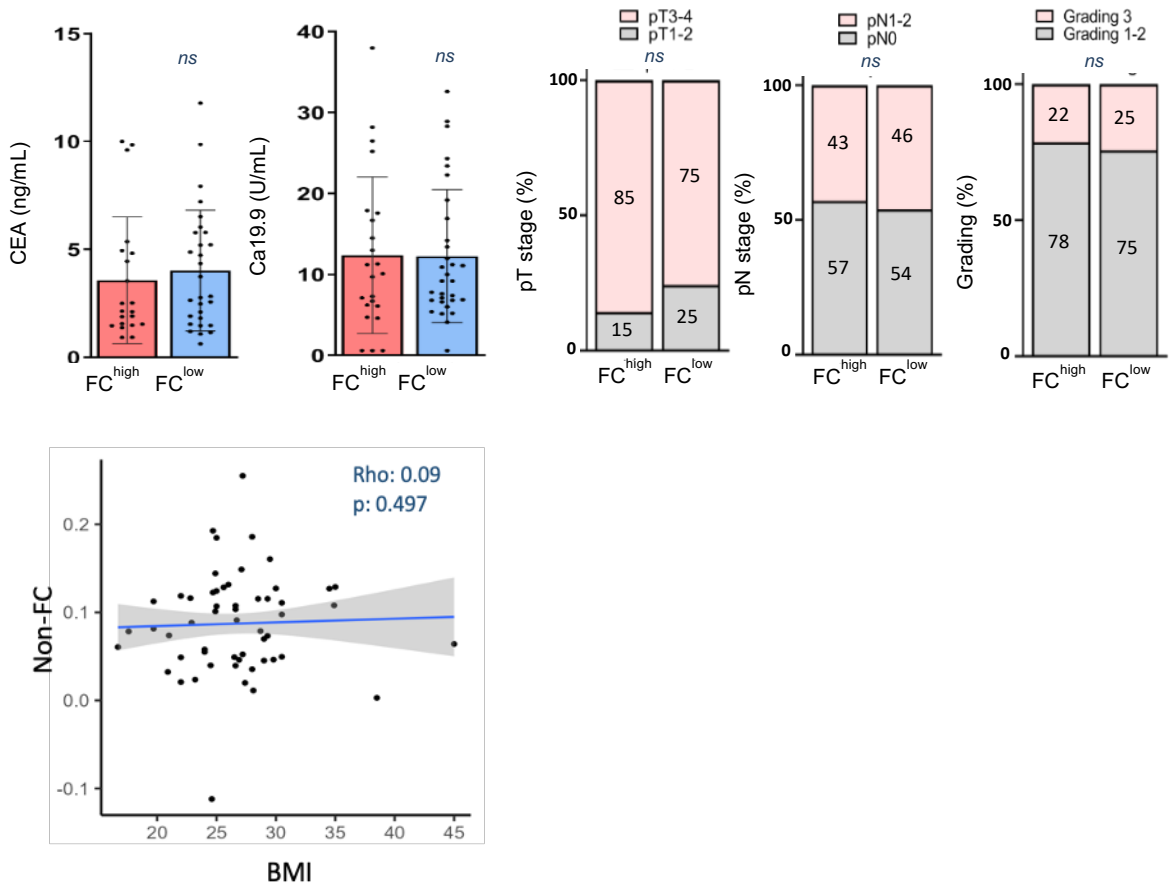

Figure S1. Relation between the abundance of FC and normal counterpart in CRC tissue, and patient's clinical and pathological variables. Graphs showing the association of CEA, Ca 19.9, pT- pN-stage and grading in FC^{high} and FC^{low} CRC. *p*-values are determined by two-tailed Mann Whitney U-test, or Fisher-exact test; *ns*, non-significant values. Correlation between BMI and non-FC was assessed by Spearman test.

Figure S2

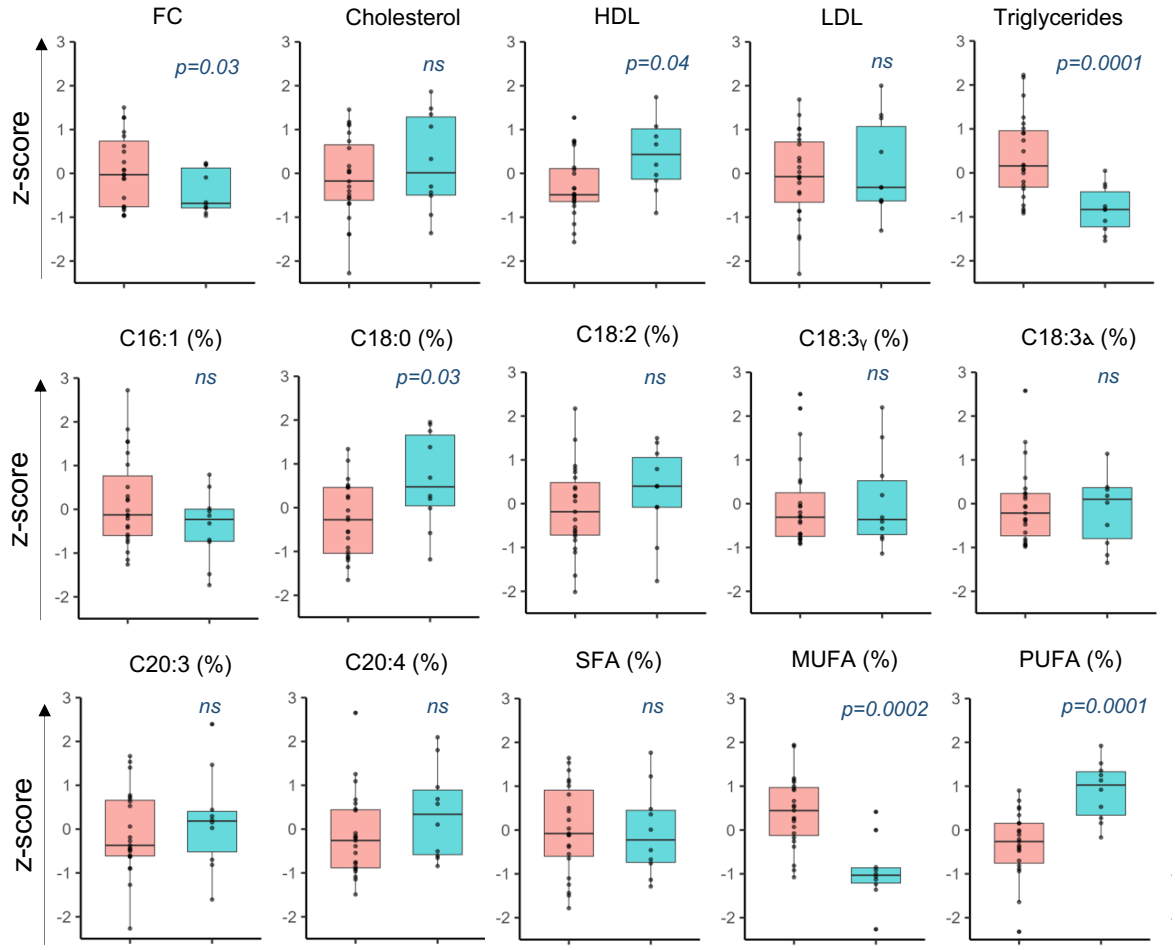

Figure S2. Association between FC and plasma lipids. Box plots of plasma lipid profile along FC^{high} and FC^{low} CRC obtained by K-means clustering method; *p*-values are determined by two-tailed Mann Whitney U-test; *ns*, non-significant values.

Figure S3

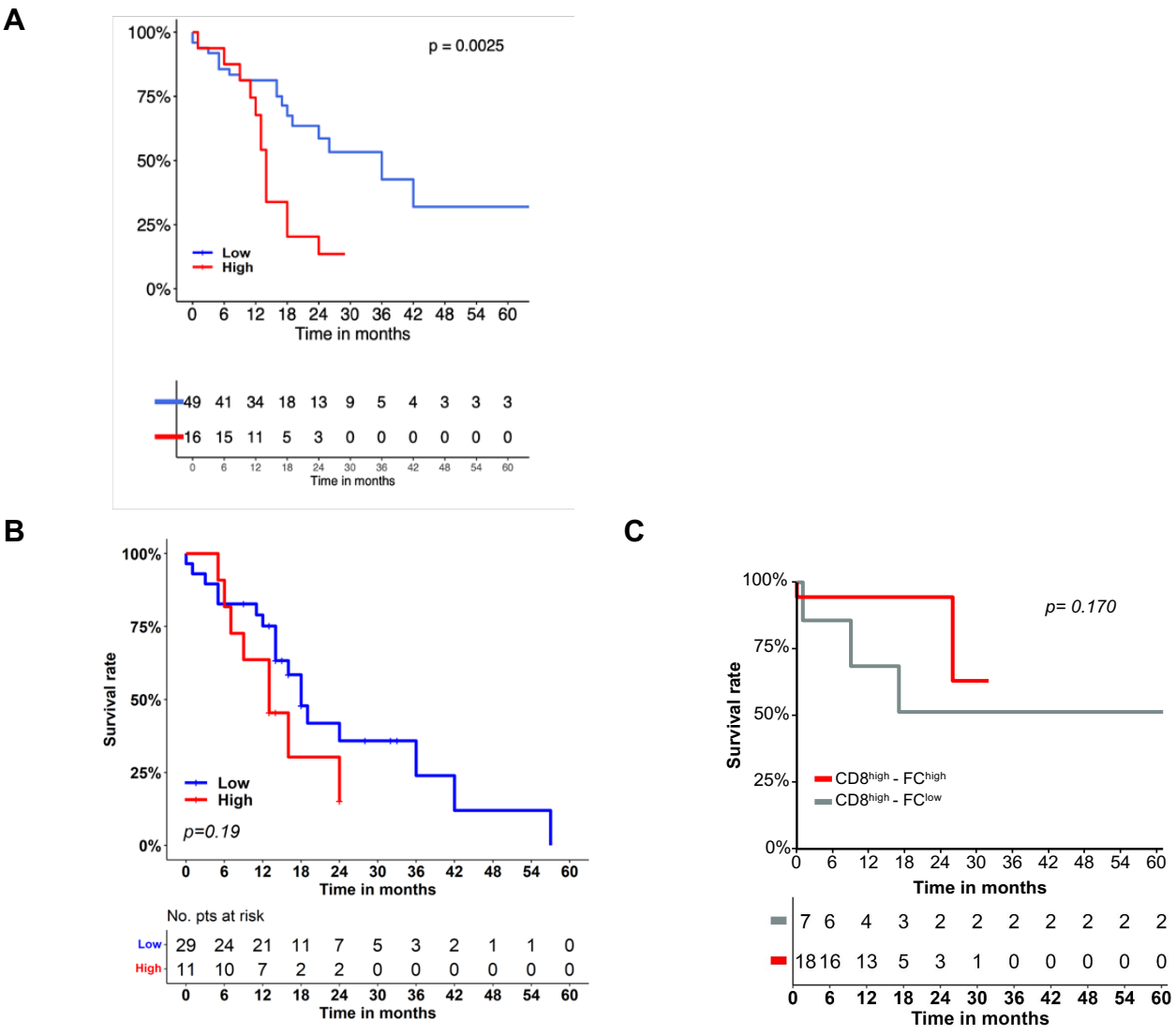

Figure S3. Disease outcome in CRC. Kaplan-Meier curves and number of patients at risk for DFS in **(A)** high vs low FC/CD8 ratio, **(B)** poor immunogenic CRC ($CD8^{low}$) classified by low and high non-FC at IM, and **(C)** high immunogenic CRC ($CD8^{high}$) stratified by FC^{high} and FC^{low} infiltrate. Log-rank *p*-values form Mantel-Cox test.

Figure S4.

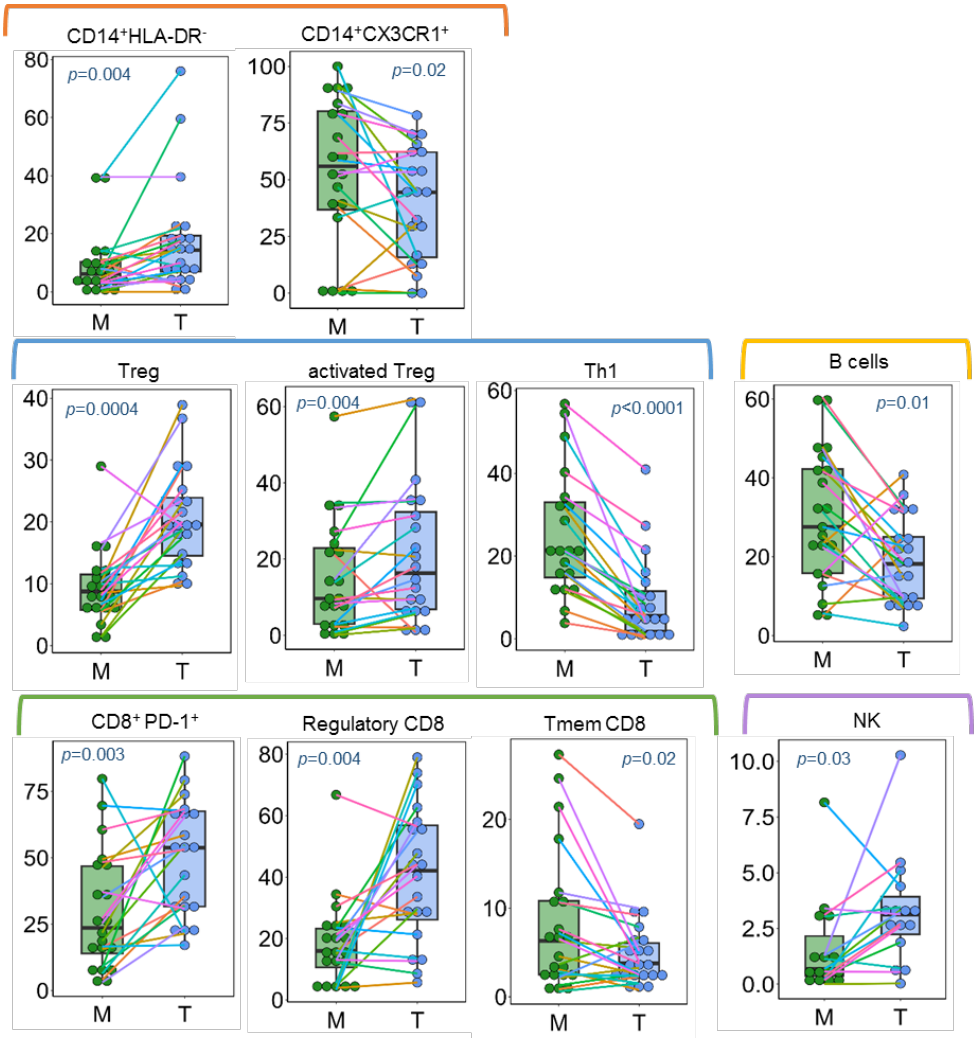

Figure S4. Immune infiltrate characterization in tissue cell suspension of stage I-III CRC. Boxplots representing the indicated cell frequencies in tumor (T) lesions and matched unaffected mucosa (M) (*n*=21). Tissues were analyzed by multiparametric flow cytometry. Statistic and *p*-values were determined by Wilcoxon signed-rank test.

Figure S5.

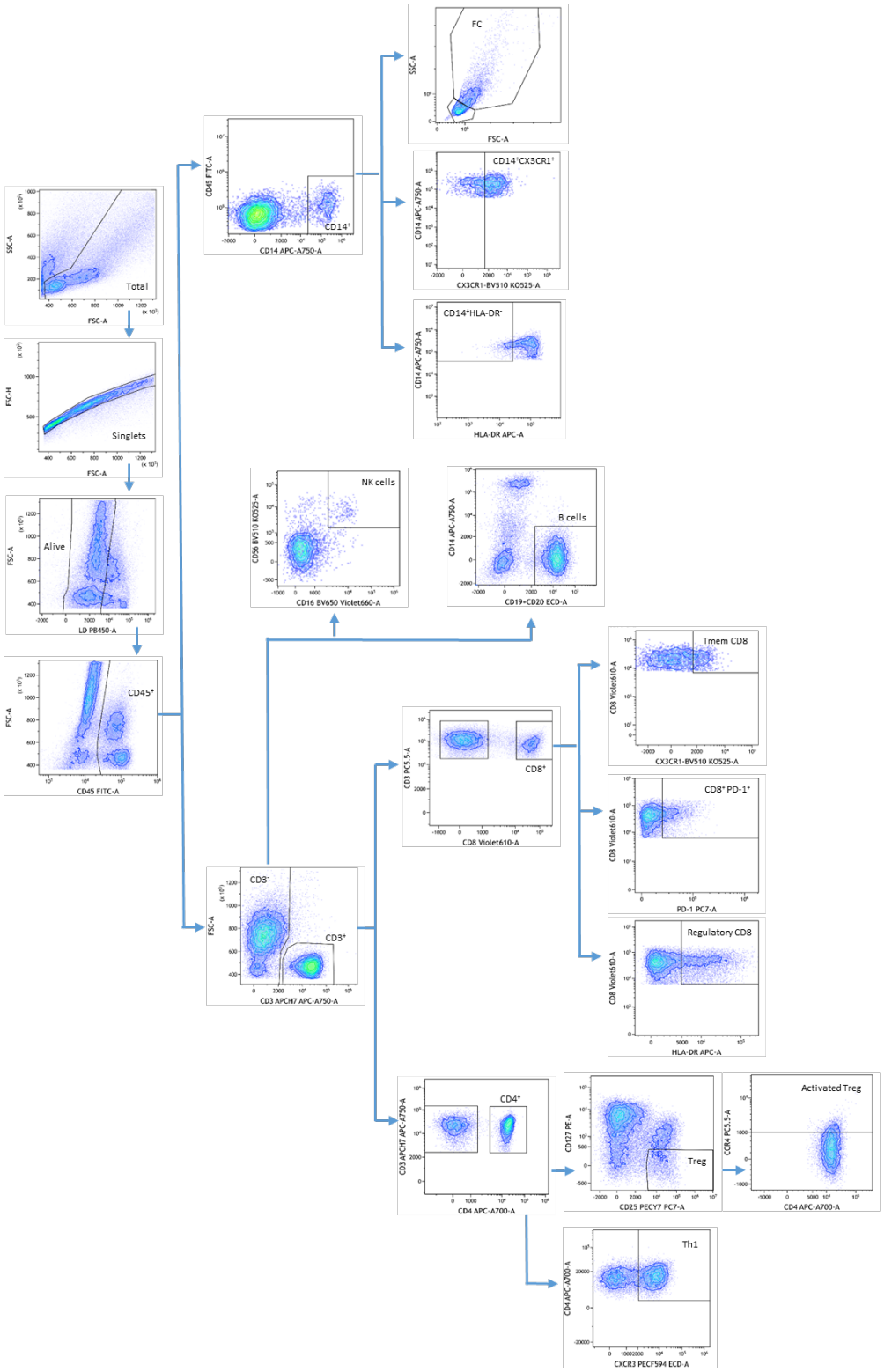

Figure S5. Representative flow cytometry gating strategies for lymphoid and myeloid population adopted in tissue cell suspension from CRC surgical specimens.

Figure S6

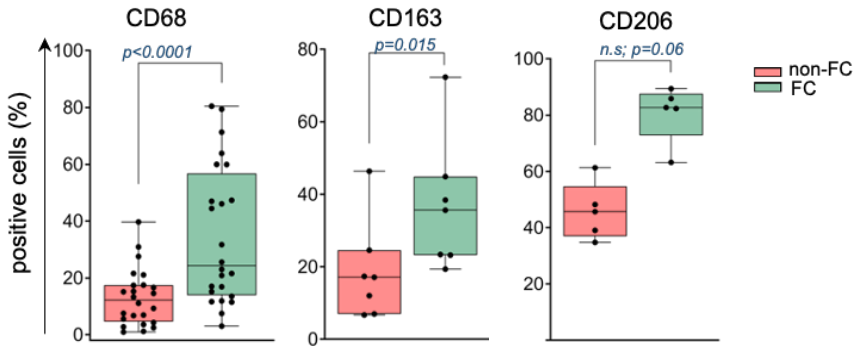

Figure S6. Immunophenotype of tissue FC and non-engulfed myeloid cells. Boxplot of CD68, CD163, and CD206 marker expression in FC and non-FC analyzed by multiparametric flow cytometry, in freshly digested tumor tissue (*n*=7-21). Statistic and *p*-values were determined by Wilcoxon signed-rank test.

Figure S7

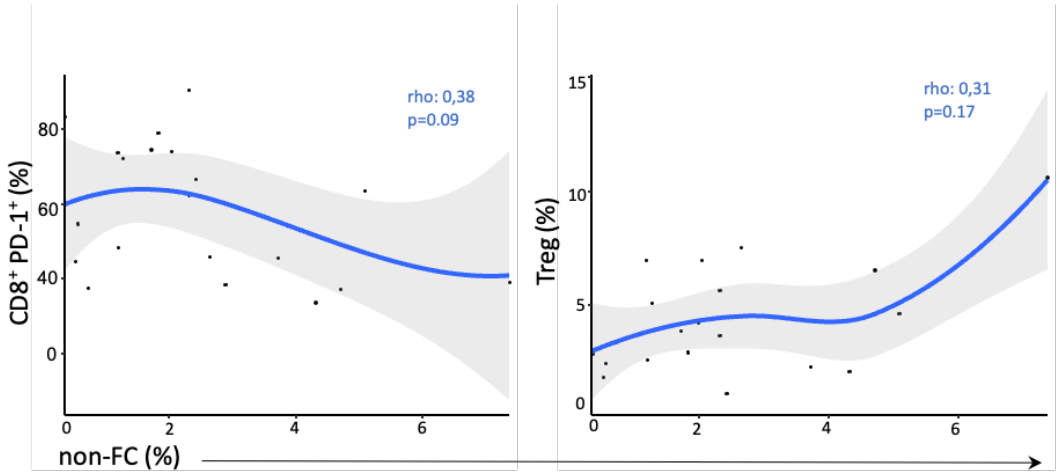

Figure S7. Correlation between the abundance of non-FC infiltrate and T-cells. Regression plots between infiltration of non-FC and activated PD-1+ CD8+ cells and Treg in freshly digested tumors (*n*=21). Spearman correlation was used to determine the *p*-value and rho coefficient.

Figure S8.

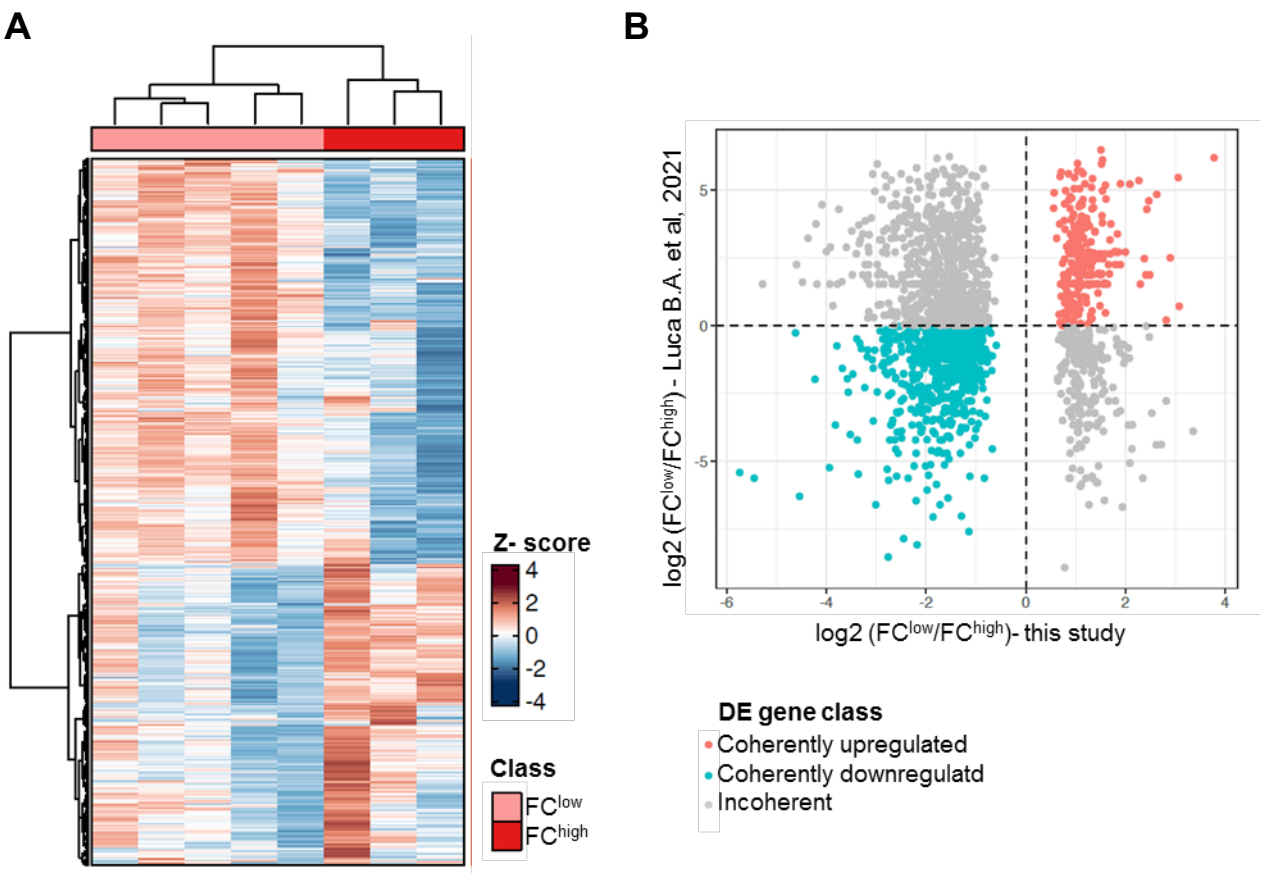

Figure S8. Differential expressed genes in colorectal tumors with high or low FC infiltration. (A) Heatmap shows the Z-score for genes that were differentially expressed in FC^{high} versus FC^{low}. **(B)** Overlap representation of Log2 fold change values according with the DE genes of micro-dissected FC-enriched CRC (Luca B.A. *et al.*, 2021) and DE genes of our study. Negative and positive coherent modulation is represented by light-blue and red dots, respectively.

Figure S9.

A

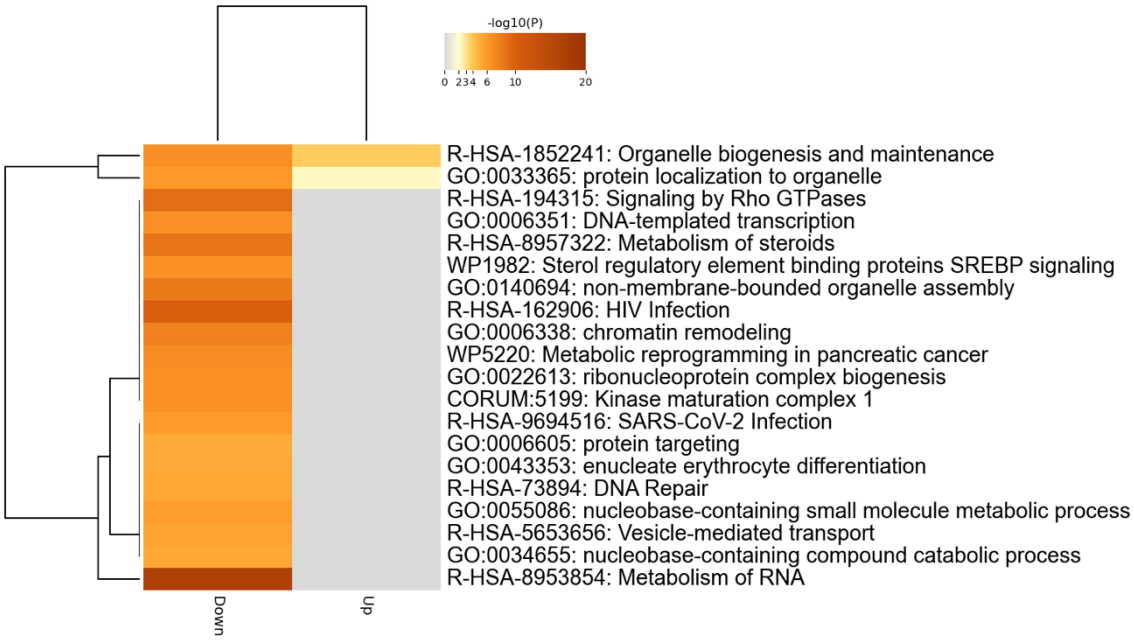

B

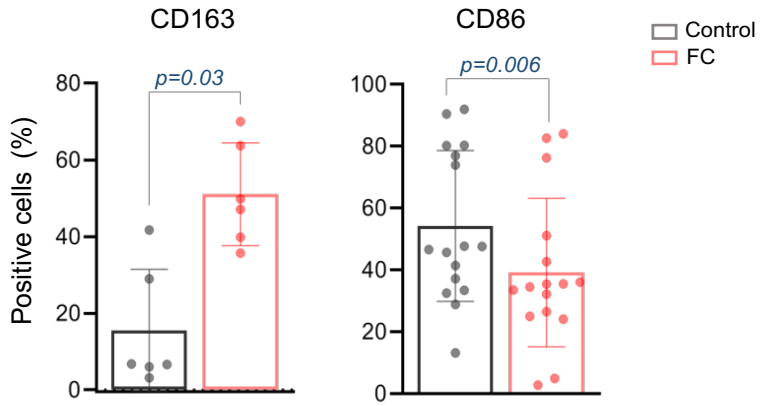

Figure S9. Function and phenotype of *in vitro*-human derived FC. **(A)** Heatmap of the top 20 significantly modulated terms identified through enrichment analysis of DE genes, coherently modulated in FC of *in vitro* and *in vivo* settings. (**B**) Flow cytometry analysis showing the percentage of positive cells for CD163 and CD86 in lipid-engulfed *in vitro* human derived macrophages, FC vs. non-engulfed controls. Statistic and *p*-values were determined by Wilcoxon signed-rank test.

Figure S10

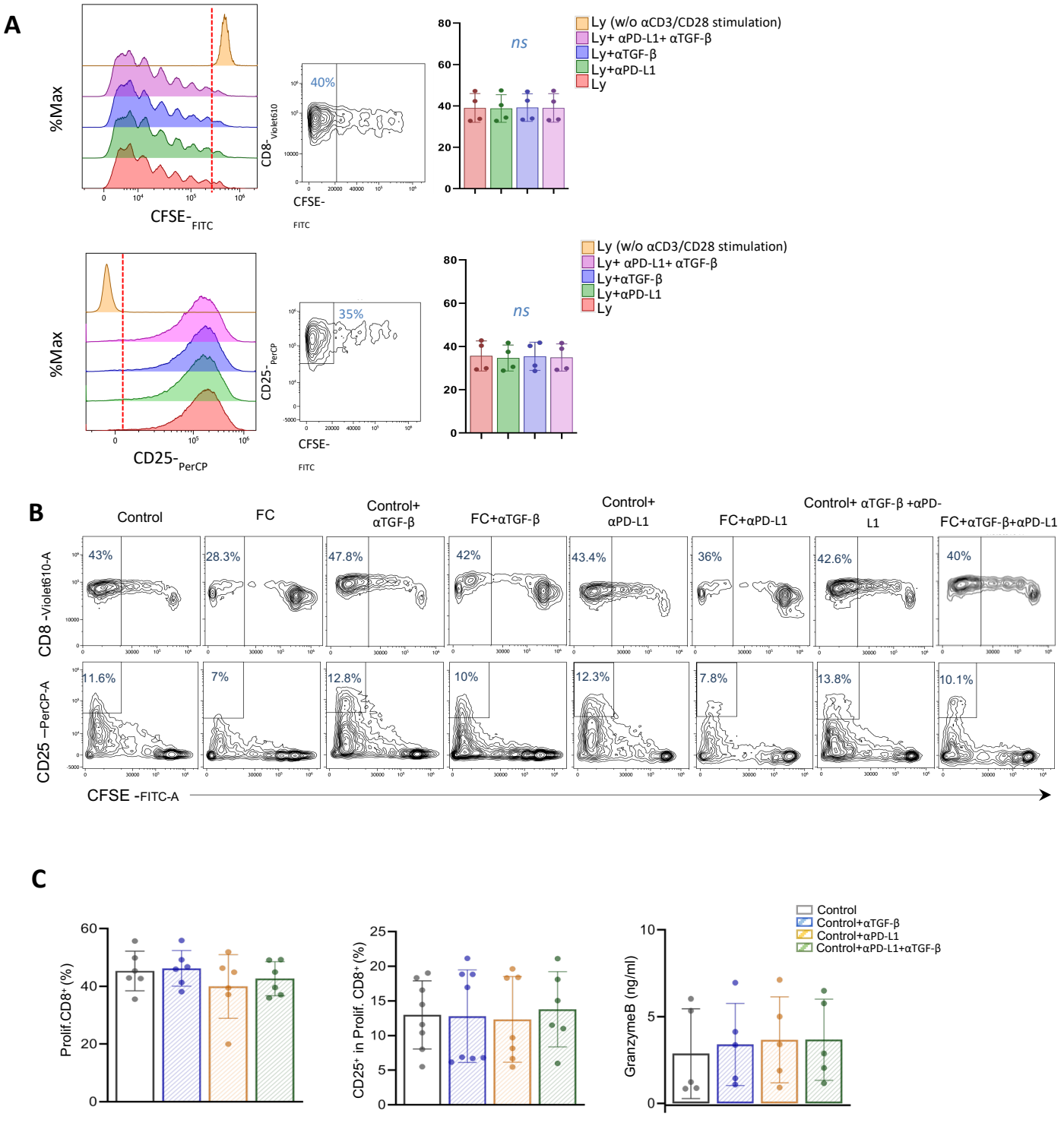

Figure S10. Proliferation and function assay in T-cells:FC co-culture. (A) CFSE staining dilution and CD25⁺ marker in proliferating CD8⁺ T-cells cultured alone for 5 days upon TCR-stimulation. Graphs show histogram of indicated marker MFI and

representative dotplots of the % of positive subsets. Non-stimulated lymphocytes (yellow peak) represent internal control. **(B)** Dot plots of T-cells: control or FC coculture (ratio 1:1), after 5 days. FC and control were 1h pretreated in presence or absence of single or simultaneously anti-TGFβ1,2,3 and anti-PD-L1 (atezolizumab) mAbs. **(C)** Boxplot of proliferating and activated ($CD25^+$) $CD8^+$ subset, as well as, GranzymeB secretion, in T-cells:control co-cultured. Statistical analysis by Friedman with Dunn's post-hoc test.

SUPPLEMENTARY TABLES

Table S1. Clinical data of CRC patients

	n= 65
Age at diagnosis (years)	69.1 (±10.8)
Gender	
Male	37 (56.9%)
Female	28 (43.1%)
BMI (Kg/m^2)	26.5 (±5.3)
Preoperative blood analyses	
CEA (ng/mL)	7.8 (±14.3)
CA 19.9 (U/mL)	14.6 (±13.0)
Neutrophil-to-lymphocyte ratio	3.7 (±4.0)
Platelet-to-lymphocyte ratio	206.5 (±120.2)
Lymphocyte-to-monocyte ratio	4.3 (±1.9)
Colorectal cancer localization	
Right-sided	18 (27.7%)
Left-sided	20 (30.8%)
Rectum	27 (41.5%)
Surgical approach	
Laparoscopy	27 (41.5%)
Laparotomy	38 (58.5%)
pT stage	
pT1-T2	13 (20.0%)
pT3	46 (70.8%)
pT4	6 (9.2%)
pN stage	
pN0	36 (55.4%)
pN1	20 (30.8%)
pN2	9 (13.8%)
Grading	
G1	1 (1.5%)
G2	49 (75.4%)
G3	15 (23.1%)
Extramural vascular invasion	
Yes	23 (35.4%)
No	42 (64.6%)
Perineural invasion	
Yes	24 (36.9%)
No	41 (63.1%)
MMR Status	
MSI	6 (9.2%)
MSS	48 (73.9%)
Not available	11 (16.9%)
Adjuvant treatment	
Chemotherapy and chemoradiation	7 (10.8%)
Chemotherapy	22 (33.8%)
None	36 (55.4%)

Table S2. List of antibodies used for IHC analysis

Antigen	Antibody clone	Supplier	Catalog number
CD8	C8/144B	Dako Agilent	M7103
CD68	KP1	Dako Agilent	M0814
CD163	10D6	Leica	NCL CD163
PD-1	D4W2J	Biocare Medical	ACI 3137
CD36	1283D	R&D	MAB19554
TGF-β	Polyclonal	Novusbio	NBP1-03276
FOXP3	259D/C7	BD Pharmigen	#560044
Ki67	MIB-1	Dako Agilent	M7240

Table S3. Reagents used for experimental analyses

Material	Supplier	Catalog	Usage
Oil red O	Abcam	ab150678	Histology
Alcian Blue PAS	Merck	A3157	Histology
Epredia™ Lab Vision UltraVision LP	Thermo Fisher	TL-125-HL	IHC
VECTASHIELD® Antifade mounting Medium with DAPI	Vectorlabs	H-1200-10	IF
HBSS	Lonza	10547F	Tissue cell suspension
EDTA	Sigma-Aldrich	03609	Tissue cell suspension
HEPES	Sigma-Aldrich	H0887	Tissue cell suspension
DTT	Sigma-Aldrich	43815	Tissue cell suspension
DNAse I	Sigma-Aldrich	10104159001	Tissue cell suspension
Collagenase D	Roche	11088866001	Tissue cell suspension
Gentamicin	Sigma-Aldrich	G1397	Tissue cell suspension
DMEM-F12	Lonza	BE12-719F	Tissue cell suspension
FBS	Euroclone	ECS0180	Tissue cell suspension/cell culture
L-glutamine	Lonza	BE17605E	Tissue cell suspension/cell culture
Pen/Strep	Lonza	DE17-602E	Cell culture
RPMI-1640	Lonza	BE12-702F	Cell culture
CD14MicroBeads, human	Miltenyi Biotec	130-050-201	Cell culture
M-CSF	Peprotech	300-25	Cell culture
ox-LDL	Invitrogen	L34357	Cell culture
DiI-oxLDL	Invitrogen	L34358	Cell culture
Bodipy 493/503	Invitrogen	D3922	Cell culture
CFSE	Invitrogen	C34554	Cell culture
Dynabeads	Gibco	11131D	Cell culture
FcR Blocking Reagent, human	Miltenyi Biotec	130-059-901	Flow cytometry
LIVE/DEAD Fixable Violet Dead Cell Stain Kit	Invitrogen	L34955	Flow cytometry
Maxwell® RSC miRNA Tissue kit	Promega	AS1460	RNA extraction
Human Soluble Protein Master Buffer Kit	BD Bioscences	558264	CBA
Human GranzymeB Flex set	BD Bioscences	560304	CBA
Human TGFβ1 Single Plex Flex Set	BD Bioscences	560429	CBA
Anti-TGF-β1,2,3 mAb	Invitrogen	MA5-23795	Cell culture
Atezolizumab (anti-PD-L1)	Tecentriq_Roche	Lot.#B0006	Cell culture

Table S4. List of antibodies used for flow cytometry analysis

Antigen	Antibody clone	Supplier	Catalog number	Fluorophore
CD3	SK7	BD PHARMIGEN	560176	APC H7
CD3	UCHT1	BD PHARMIGEN	560835	PerPC-Cy5.5
CD3	UCHT1	BECKMAN COULTER	B00068	KrO
CD4	RTA-T4	BD PHARMIGEN	557922	Alexa700
CD4	SK3	BD BIOSCIENCE	562970	BV510
CD25	M-A251	BD PHARMIGEN	557741	PE-Cy7
CCR4	1G1	BD PHARMIGEN	560726	PerCP-Cy5.5
CCR6	11A9	BD BIOSCIENCE	563241	BV 510
CCR7	3D12	BD BIOSCIENCE	557734	Alexa647
CCR10	1B5	BD PHARMIGEN	564771	APC
CXCR3	1C6/CXCR3	BD BIOSCIENCE	562451	PECF-594
CD127	R34.34	BECKMAN COULTER	B49220	PE
CD45	HI30	BD PHARMIGEN	555482	FITC
CD45	HI30	BD BIOSCIENCE	563204	BV510
CD45RA	HI100	BD BIOSCIENCE	555488	FITC
EpCAM	HEA125	MILTENYI BIOTEC	130-113-264	PE
CD8	SK1	BIOLEGEND	344742	BV605
PD-1	PD1.3	BECKMAN COULTER	A78885	PC7
PD-L1	MIH1	BD BIOSCIENCE	563742	PECF-594
CD14	RM052	BECKMAN COULTER	A86052	Alexa750
CX3CR1	2A9-1	BD BIOSCIENCE	744487	BV510
CX3CR1	2A9-1	BD BIOSCIENCE	744488	BV605
HLA-DR	Immu-357	BECKMAN COULTER	Im3635	APC
CD68	EBioY1/82A	eBIOSCIENCE	12-0689-71	PE
CD11b	Bear1	BECKMAN COULTER	A54822	PC7
CD33	WM53	BD PHARMIGEN	561160	Alexa700
CD33	D3HL60.251	BECKMAN COULTER	A70198	PC5.5
CD19	J3-119	BECKMAN COULTER	A07770	ECD
CD20	B9E9	BECKMAN COULTER	B92433	ECD
CD25	B1.49.9	BECKMAN COULTER	B92458	PC5.5
CD56	NCAM16.2	BD BIOSCIENCE	563041	BV510
TCRγδ	B1	BD PHARMIGEN	555717	PE
CD86	2331(FUN-1)	BD PHARMIGEN	555658	PE
CD163	GHI/61	BD PHARMIGEN	563887	PerCP-Cy5.5
CD206	15-2	BIOLEGEND	321104	FITC

Abbreviations: IHC, immunohistochemistry; IF, immunofluorescence, CBA, cytometric bead array;

Table S5. RNA_seq analysis. Table is provided as .xlsl file.

Table S6. BMI association with clinical-pathological variables

	Rho	*p value*
Age at diagnosis	0.125	0,364
CEA	0.090	0,536
Ca19.9	0.097	0,508
NLR	0.071	0,605
PLR	-0.162	0,237
LMR	-0.214	0,115

Rho: Spearman correlation (*p<0.05);

	Mean (± SD)	*p value*
Gender		0,9395
Male	27.18 (± 5.4)	
Female	26.18 (± 4.3)	
Colorectal cancer localization		0,7039
Right side	27.19 (± 6.1)	
Left side	26.51 (± 4.4)	
pT stage		0,5556
T1-T2	27.5 (± 4.5)	
T3-T4	26.53 (± 5)	
pN stage		0,3083
N0	26.1 (± 3.6)	
N1-N2	27.48 (± 6.1)	
Grading		0,7443
G1-G2	26.5 (± 4.3)	
G3	27.5 (± 6.7)	
Extramural Vascular invasion		0,2436
Yes	27.38 (± 5.2)	
No	26.4 (± 4.8)	
Perineural Invasion		0,4245
Yes	27.14 (± 5.1)	
No	26.5 (± 4.8)	
MRR status		0,9657
MSS	26.99 (± 5)	
MSI	25.95 (± 5.1)	
Adjuvant treatment		0,8253
Yes	26.61 (± 5.7)	
No	26.78 (± 4.3)	

Statistic: Mann-Whitney test (*p<0.05);

Table S7. Univariate analysis of the clinical and pathological factors associated with DFS of CRC patients within the cohort study.

	Univariate analysis		
	HR	95%CI	p-value
Age at diagnosis	1.29	0.75-2.21	0.357
BMI (kg/m^2)			
Low	ref	ref	ref
High	1.71	0.63-4.65	0.287
CEA	1.14	1.05-1.23	**0.002***
CA19.9	1.57	1.15-2.14	**0.004***
NLR			
Low	ref	ref	ref
High	2.07	1.03-4.16	**0.042***
pT stage			
pT1-2	ref	ref	ref
pT3-4	2.15	0.74-6.19	0.158
pN stage			
pN0	ref	ref	ref
pN1-2	1.42	0.70-2.86	0.327
Grading			
G1-G2	ref	ref	ref
G3	1.35	0.60-3.03	0.470
Extramural vascular invasion			
No	ref	ref	ref
Yes	2.55	1.25-5.19	**0.010***
Perineural invasion			
No	ref	ref	ref
Yes	2.12	1.04-4.32	**0.038***
Microsatellite status			
MSS/pMMR	ref	ref	ref
MSI/dMMR	0.86	0.20-3.70	0.841
Adjuvant chemotherapy			
No	ref	ref	ref
Yes	1.77	0.87-3.63	0.117
Type of immune infiltrate			
FC^{low} $CD8^{low}$	ref	ref	ref
FC^{high} $CD8^{low}$	2.48	1.10-5.56	**0.03***
$CD8^{high}$	0.30	0.11-0.78	**0.013***

Abbreviations: HR, hazard ratio; CI, confidence interval;Statistic: Cox proportional hazard regression models; *statistically significant ($p<0.05$).

2. MATERIAL AND METHODS

2.1. Human studies

Prospective and retrospective cohort of CRC patients (*n*=65) with sporadic colorectal cancer treated by upfront surgery between 2009 and 2021 at the colorectal Surgery unit of Fondazione IRCCS Istituto Nazionale dei Tumori, were accrued in this study. The protocols were approved by the Ethical Committee (INT127/19 and INT149/2019) and were conducted in compliance with the Declaration of Helsinki. All participants gave informed written consent for the study. Enrolled CRC patients were histological-confirmed T2-T4 with any N stage, and any microsatellite stability status. Indication for neoadjuvant chemotherapy or immunosuppressive medication within the last 6 months prior surgery were considered as criteria for exclusion from the study. The main clinical characteristics were summarized in **Supplementary Table S1**. Survival time included overall survival (OS) defined as the time from surgery to death or the last follow-up date, and disease free survival (DFS) indicating the time from surgery to any first event, either distant metastasis or local relapses.

2.2. Biological sample

Fresh primary CRC tissue with matched healthy mucosa collected at ≥ 10 cm distance from tumor (*n*=21), were collected from the prospective cohort. Tissue samples were freshly processed for single cell suspension and collected for histopathological analyses, either OCT embedded and frozen or formalin fixed and paraffin-embedded (FFPE). FFPE tissue sections were also collected from the retrospective case set.

Peripheral blood mononuclear cells (PBMCs) from CRC patients and healthy donors were collected and processed for CD14+ cell sorting for further *in-vitro* analyses.

2.3. Immunohistochemistry and Immunofluorescence

Pathological evaluations were made on Hematoxylin-Eosin (EE) and Alcian Blue PAS staining on FFPE tissue sections. Oil-Red-O (Abcam, Cambridge, UK) staining was processed on OCT- embedded tissue sections. For immunohistochemical (IHC) analyses, sections were stained with antibodies detailed in **Supplementary Table S2**. Briefly, sequential 3 µm-thick slides were, cut from FFPE samples, dried, de-waxed, rehydrated, and unmasked (with Dako PT-link, EnVision™ FLEX Target Retrieval Solution, High/Low pH). Primary antibodies were incubated with a commercially available detection kit (EnVision™ FLEX+, Dako, Denmark) in an automated Immunostainer (Dako Immunostainer Link 48). Positive and negative sections were adequately included. High resolution images were captured using Aperio Scanscope XT (Aperio), at 40X magnification.

For immunofluorescence staining, after antigen retrieval, samples were treated briefly with 0.1 M glycine in phosphate buffered saline (PBS) pH 7.4 followed by a buffer with 0·3% Triton X-100 and incubated overnight at 4°C with the primary antibodies, then washed and incubated for 1 h with appropriate conjugated secondary antibodies (**Supplementary Table S2**). Slides were mounted on glass slides with 95% glycerol in PBS. Epifluorescence scanning images were acquired using a motorized Olympus BX63 fluorescence microscope equipped with the X-cite 120 fluorescence illumination system (EXFO, Quebec, Canada), DP80 camera and software cellSens (Shinjuku Monolith, Tokyo, Japan). Nuclei were stained with 4′,6-diamidino-2-phenylindole (DAPI, Vectorlabs, Newark, CA, USA). Confocal microscopy was carried out using a Zeiss LSM 710 confocal microscope (GmbH 07745; Jena, Germany) equipped with a

458-, 488-, 514-nm multiline argon laser, 561-nm diode pumped solid state laser and a 633-nm HeNe laser.

2.4. Digital imaging analysis

Digitally scanned sections were annotated with ImageScope software (Aperio Technologies, Leica Microsystem, Wetzlar, Germany). Considering the high variability in size and range of tumor islets and stroma, image annotation was manually outlined by an experienced pathologist. Tumor core (TC), invasive margin (IM) and adjacent mucosa (AM) region were manually annotated excluding from the analysis the areas of necrosis, artifacts, tissue fold and germinal centers. Therefore, the image colors were deconvoluted from chromogen DAB to RGB color model, enabling a visual output of the various immune markers within the tissue. Imaging segmentation, including marker-pixel density and location was performed with MIAQuant and MIAQuant_Learn as previously described (1,2), on the whole tissue section. The software uses a User-interface to allow expert users to provide few examples of marked and not-marked tissue areas. The provided examples are used to train a stacked classifier that is then applied to all the images to identify, localize, and quantify markers. Once the markers have been identified in the tissue, given the user provided IM (50μm thick band), the density of all the marker areas are identified in peri-tumoral (peri) and intra-tumoral bands (intra) with increasing width of 400 μm from the IM. TC was defined as the remaining intra-tumoral area with an extent of 1200 μm from the IM, while AM has been considered as the healthy mucosa external to the IM, with an extent of 2000 μm.

Next, the marked cells where automatically filtered to only keep larger macrophages, that is macrophages with an area greater than 20 μm^2.

Given the output of MIAQuant_Learn, all the filtering and analysis code was implemented with MATLAB R2021b coding environment.

2.5. Intestinal tissue specimens

Collected surgical specimens were placed in HBSS (Lonza, Thermo Fisher, Waltham, MA, USA) containing 5 mM EDTA (Sigma-Aldrich, Merck Life Science, Darmstadt, Germany), 5% FBS (Euroclone, Milan, Italy), 50 ng/mL gentamicin (Sigma-Aldrich), 10 mM HEPES (Sigma-Aldrich) and 1 mM DL-Dithiothreitol (DTT, Sigma-Aldrich) at 37°C for 30 min under rotation condition. The digested tissues were passed through a 70 µm cell strainer (Miltenyi Biotec, Bergisch Gladbach, Germany), pelleted and kept at 4°C in DMEM-F12 (Lonza) supplemented with 50 ng/ml gentamicin and 10% FBS. This step was repeated for three times. The remaining fragments, were incubated in complete DMEM-F12 with 2 mg/ml Collagenase D (Roche, Merck Life Science, Darmstadt, Germany) and 1000 U/ml DNase I (Sigma-Aldrich) at 37°C for 30 min under rotation condition. Afterwards, the cell suspension was filtered throughout a 70 µm cell strainer. The filtered single cell suspensions were pooled for subsequent flow cytometry analyses.

2.6. Monocyte studies

Monocytes (purity >95%) were purified from PBMCs of HD and CRC patients by sorting with anti-$CD14^+$ beads (MACS, Miltenyi Biotec) according to the manufacturer's instructions. Isolated $CD14^+$ monocytes were cultured with RPMI-1640 (Lonza) supplemented with 10% fetal bovine serum (FBS, Euroclone), 100 U/ml penicillin and 100µg/ml streptomycin (Lonza), and 24mM glutamine (Lonza). Monocyte-derived macrophages were generated by culturing sorted $CD14^+$ cells in complete medium with 50 ng/ml macrophage colony-stimulating factor (M-CSF, PeproTech, ThermoFisher, Waltham, MA, USA), in absence or presence of 50 µg/ml oxidized low-density lipoprotein (oxLDL, Invitrogen, ThermoFisher) for 48 h. Lipid uptake was determined

by flow cytometry after incubation with 10-75 µg/ml Dil-labeled oxLDL (Invitrogen) or oxLDL followed by incorporation of 1 µM BODIPY$^{493/503}$ (Invitrogen). For proliferation studies, CD14^{-} enriched fraction were stained with 5 µM CFSE (Invitrogen) prior stimulation with 12x10^{4} anti-CD3/anti-CD28 mAbs-conjugated beads each 10^{6} cells (Dynabeads™ Human T-Activator CD3/CD28, Gibco, ThermoFisher) for 5 h. Then, T cells were co-cultured with early macrophages treated with or without oxLDL, in presence or absence of single and/or simultaneously treatment with 1.25µg/ml anti-TGF1,2,3, and 50µg/ml anti-PD-L1 (atezolizumab) mAbs. Co-cultures were performed at the ratio 1:1 for 5 days to assessed T-cell proliferation and phenotype by multiparametric flow cytometry. Culture of lymphocytes alone were used as internal reference. Cytometric Bead Array (CBA) (BD Bioscience, Franklin Lakes, NJ, USA) was used to assess cytokine concentration in cell culture supernatant and determined cytokine concentration were normalized by the number of cell/condition . Reagents have been listed in **Supplementary Table S3**.

2.7. Flow cytometry

Immunophenotyping studies were performed on tissue single cell suspension, and *in vitro* stimulated cells by 13-multicolor flow cytometry (Cytoflex S, Beckman Coulter, Brea, CA, USA). Briefly, cells were incubated with live/dead (Thermo Fisher Scientific) staining for 30 min on ice and washed. Samples were treated with Fc blocking reagent (Miltenyi Biotec) for 10 min at RT, and subsequently incubated with different mAbs, listed in **Supplementary Table S4**, for 30 min at 4°C. Thereafter, samples were washed, fixed and acquired on a Cytoflex S. Among CD4 cell population, Treg were identified as CD4^{+}CD25^{+}CD127^{-} while activated Treg expressed CCR4^{+}; Th1 subpopulation included CD4^{+}CXCR3^{+} cells. Among CD8 T lymphocytes, cells

expressing HLA-DR were identified as regulatory CD8, while $CX3CR1^+$ cells identified Tmem CD8 cluster. Among $CD3^-$ population, B cells were identified as $CD19^+CD20^+$ and NK as $CD56^+$ $CD16^+$ cells. For tissue cell suspension, unsupervised analysis of flow cytometry data was performed using uniform manifold approximation and projection (UMAP) algorithm using RStudio and Cytobank (Beckman Coulter). After setting the compensation matrix, $CD45^+$ events were extracted, and logical transformation was applied. UMAP analysis was achieved on 38.560 $CD45^+$ cells for each sample. Supervised analysis was performed using Kaluza Software (Beckman Coulter) on flow cytometry data of tissue cell suspension and *in vitro* studies. Gating strategies for myeloid and lymphoid cells are depicted in **Supplementary Figure S5**.

2.8. Lipidomics analysis

Whole blood samples were collected in 10 mL Vacutainer tubes with spray-coated K_2EDTA. Plasma was separated by 2 centrifugations at 1300 x g at RT for 10 min and held at -80°C until use. Cobas Roche automated clinical chemistry analyzed (Roche Diagnostic) was used to determine total cholesterol, HDL, LDL and triglycerides following the standard clinical procedures. Plasma esterified fatty acids (EFAs) were analyzed as methylesters after derivatization with sodium methoxide in methanol 3.33% (w/v) and extraction with hexane. Prior to derivatization a known amount of internal standard (C17:0 triglyceride) was added to each sample to correct for yield and recovery of the reaction. EFAs were injected into a capillary gas chromatograph (Shimadzu GC-2025) equipped with flame ionization detector. The separation was achieved with capillary Zebron FAME, length 30 m x 0.25 mm I.D., film thickness 0.20 μm; carrier gas, helium; injector temperature, 250°C; detector temperature, 275°C; oven temperature, 100°C for 2 min and then increased at rate of 10°C min^{-1} to 250°C..

A standard mixture containing all fatty acid methylesters (Sigma Aldrich, MO) was injected for calibration. Fatty acid methyl esters were quantified using the chromatographic peak area according to the internal standard (IS) method (3).

2.9. Transcriptomic analysis

CRC specimens with high or low FC content based on H&E staining and in-vitro lipid-engulfed macrophages were analyzed by bulk RNAseq.

RNA from CRC and FAP FFPE samples was extracted using Maxwell® RSC miRNA tissue kit on Maxwell® RSC Instrument (Promega, Madison, WI, USA) (**Supplementary Table S3**). The RNA concentration of each sample was assessed with a Qubit 4 fluorometer (Thermo Fisher Scientific Inc., Waltham, MA, USA) using the Qubit RNA BR Assay (Thermo Fisher Scientific Inc.). RNA purity was assessed as 260/280 and 260/230 ratios by spectrometric analysis on a Tecan Spark® multi-mode microplate reader (Tecan Trading AG, Switzerland).

RNA integrity was verified by electrophoretic run on a 2100 bioanalyzer (Agilent Technologies, Santa Clara, CA, USA) loaded with an RNA 6000 Nano Chip. Total RNA libraries were prepared with the Illumina Stranded Total RNA Prep with Ribo-Zero Plus kit (Illumina Inc., San Diego, CA, USA), according to the manufacturer's instructions without any modification of the protocol.

The size and quality of the final libraries were assessed by electrophoretic run on the Bioanalyzer 2100 using a High Sensitivity DNA Chip. The concentration of each library was measured with a High Sensitivity (HS) Assay on a Qubit 4 fluorometer. Individual libraries were then pooled in an equimolar manner into a single pool, and the pool was diluted to a final concentration of 1.4nM.

The pool with the addition of 1% PhiX spike-in was then sequenced on a

NovaSeq6000 sequencer (Illumina Inc), using an S2 v1.5 flow cell, with a 2x100 pair-end protocol.

Sequencing reads were preprocessed with fastp v0.21.0 4 (4) in default settings to remove reads associated with a low quality (phred quality <Q15), shorter than 15 nt reads, or with more than 5 Ns. Reads passing the filtering step were aligned to the human Gencode v36 transcriptome using Salmon v1.4.0 (5) with option --validateMappings, --seqBias, and --gcBias. Transcripts Per Million (TPM) gene expression matrices were obtained using tximport v1.18.0 (6) R package.

2.10. Bioinformatic tools

Differential expression analysis was performed using the DESeq2 v1.30.1 R package (7). A gene was defined as differentially expressed (DE) if associated with and adjusted p-value < 0.05 and TPM > 1 in all analysed sample classes.

The comparison between FC^{high} and FC^{low} CRC form Luca B.A. et al. 2021 (8) was performed by retrieving the expression levels from the publication and by computing the log2 fold-change of gene expression computed FC^{high} and FC^{low} tumors. Gene set functional enrichment analysis was performed with metascape v3.5 in default settings (9). A term was considered significantly enriched if associated with an adjusted p-value < 0.001. Scoring of custom gene signatures from literature was performed using singscore v1.10 (10). Transcript profiles and data sets used for RNAseq have been uploaded to the GEO under the Super Series accession number GSE227206 and GSE273106 . Detailed information are described in Supplementary **Table S5**.

2.11. Statistical analyses

Standard descriptive statistics (absolute and relative frequencies for categorical variables, mean ± SD for continuous variables) were used to describe the sample characteristics. The non-parametric Wilcoxon Mann-Whitney test, two-way ANOVA or Fisher-exact test were applied as specified to compare the distribution of the variables. Correlation analyses associated the expression of different cell populations in tissue and represented through a bivariate scatterplot. Spearman's test was applied.

Maximally selected log-rank statistics was used to investigate the optimal cut-off values for CD8+, CD68+ FC and non-FC cells. Kaplan-Meier curves and the Log-rank test were used to analyze DFS.

Prognostic factors were investigated by univariate analyses using the Cox proportional hazard regression models. The conventional two-sided 5 percent level was chosen as the threshold of statistical significance. Statistical analyses and graphical representation were performed with R software (version 4.2.0, R Foundation for Statistical Computing, Vienna, Austria) and GraphPad Prism 8.4.3.

Supplementary methods references

1. Casiraghi E, Cossa M, Huber V, Rivoltini L, Tozzi M, Villa A*, et al.* MIAQuant, a novel system for automatic segmentation, measurement, and localization comparison of different biomarkers from serialized histological slices. Eur J Histochem **2017**;61(4):2838 doi 10.4081/ejh.2017.2838.
2. Casiraghi E, Huber V, Frasca M, Cossa M, Tozzi M, Rivoltini L*, et al.* A novel computational method for automatic segmentation, quantification and comparative analysis of immunohistochemically labeled tissue sections. BMC Bioinformatics **2018**;19(Suppl 10):357 doi 10.1186/s12859-018-2302-3.
3. Perrotta S, Roberti D, Bencivenga D, Corsetto P, O'Brien KA, Caiazza M*, et al.* Effects of Germline VHL Deficiency on Growth, Metabolism, and Mitochondria. N Engl J Med **2020**;382(9):835-44 doi 10.1056/NEJMoa1907362.
4. Chen S, Zhou Y, Chen Y, Gu J. fastp: an ultra-fast all-in-one FASTQ preprocessor. Bioinformatics **2018**;34(17):i884-i90 doi 10.1093/bioinformatics/bty560.
5. Patro R, Duggal G, Love MI, Irizarry RA, Kingsford C. Salmon provides fast and bias-aware quantification of transcript expression. Nat Methods **2017**;14(4):417-9 doi 10.1038/nmeth.4197.
6. Soneson C, Love MI, Robinson MD. Differential analyses for RNA-seq: transcript-level estimates improve gene-level inferences. F1000Res **2015**;4:1521 doi 10.12688/f1000research.7563.2.
7. Love MI, Huber W, Anders S. Moderated estimation of fold change and dispersion for RNA-seq data with DESeq2. Genome Biol **2014**;15(12):550 doi 10.1186/s13059-014-0550-8.

8. Luca BA, Steen CB, Matusiak M, Azizi A, Varma S, Zhu C*, et al.* Atlas of clinically distinct cell states and ecosystems across human solid tumors. Cell **2021**;184(21):5482-96 e28 doi 10.1016/j.cell.2021.09.014.

9. Zhou Y, Zhou B, Pache L, Chang M, Khodabakhshi AH, Tanaseichuk O*, et al.* Metascape provides a biologist-oriented resource for the analysis of systems-level datasets. Nat Commun **2019**;10(1):1523 doi 10.1038/s41467-019-09234-6.

10. Bhuva DD, Cursons J, Davis MJ. Stable gene expression for normalisation and single-sample scoring. Nucleic Acids Res **2020**;48(19):e113 doi 10.1093/nar/gkaa802.